Fawwaz et al., *BioImpacts.* 2024;14(1):27774
doi: 10.34172/bi.2023.27774
https://bi.tbzmed.ac.ir/

Synthesis and initial *in vitro* evaluation of olmutinib derivatives as prospective imaging probe for non-small cell lung cancer

Muammar Fawwaz[1,2*], Kenji Mishiro[3*], Arwansyah[4], Ryuichi Nishii[5], Kazuma Ogawa[2,3*]

[1]Laboratory of Pharmaceutical Chemistry, Faculty of Pharmacy, Universitas Muslim Indonesia, Urip Sumoharjo KM. 5, Makassar 90-231, Indonesia
[2]Graduate School of Medical Sciences, Kanazawa University, Kakuma-machi, Kanazawa, Ishikawa 920-1192, Japan
[3]Institute for Frontier Science Initiative, Kanazawa University, Kakuma-machi, Kanazawa, Ishikawa 920-1192, Japan
[4]Department of Chemistry Education, Faculty of Teacher Training and Education, Universitas Tadulako, Palu, Indonesia
[5]Biomedical Imaging Sciences, Department of Integrated Health Sciences, Graduate School of Medicine, Nagoya University, Higashi-ku, Nagoya 461-8673, Japan

Article Info

Article Type:
Original Article

Article History:
Received: 16 Jan. 2023
Revised: 18 Jul. 2023
Accepted: 5 Aug. 2023
ePublished: 19 Aug. 2023

Keywords:
Cytotoxicity
L858R/T790M
Molecular docking
Tyrosine kinase inhibitor

Abstract

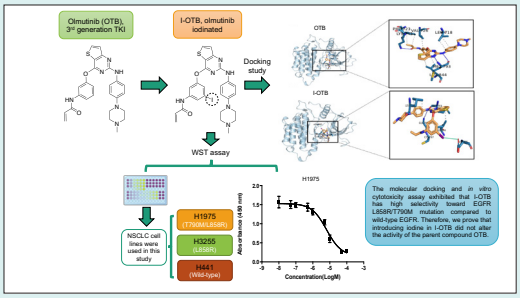

Introduction: Imaging a non-small cell lung cancer (NSCLC) using radiolabeled tyrosine kinase inhibitors (TKIs) has attracted attention due to their unique interaction with the target epidermal growth factor receptor (EGFR). Olmutinib (OTB) is one of the third-generation EGFR TKIs, which selectively inhibit EGFR L858R/T790M mutation. In this study, we aim to estimate the interaction of the iodinated OTB (I-OTB)-receptor complex by molecular docking. Furthermore, we will synthesize the I-OTB and evaluate its activity toward EGFR L858R/T790M by *in vitro* cytotoxicity assay.

Methods: A molecular docking simulation was carried out using an AutoDock Vina program package to estimate the interaction of the ligand-receptor complex. The I-OTB, *N*-{3-iodo-5-[(2-{[4-(4-methylpiperazin-1-yl)phenyl]aminothieno{3,2-d}pyrimidin-4-yl)oxy]phenyl} acrylamide, was synthesized by introducing an iodine atom in the phenyl group in the 3-aryloxyanilide structure. The half inhibitory concentration (IC_{50}) was determined by employing a 2-(2-methoxy-4-nitrophenyl)-3-(4-nitrophenyl)-5-(2,4-disulfophenyl)-2H tetrazolium monosodium salt (WST-8) assay to evaluate the activity of I-OTB.

Results: The docking study exhibited that I-OTB could take an interaction similar to that of the parent compound. We successfully synthesized I-OTB and confirmed its structure by instrumental analysis. The binding energy of OTB and I-OTB in complex with EGFR T790M are -8.7 and -7.9 kcal/mol, respectively. The cytotoxicity assay showed that I-OTB also has an affinity towards the EGFR L858R/T790M mutation with the IC_{50} 10.49 ± 5.64 μM compared to the EGFR wild type with the IC_{50} over than 10 μM.

Conclusion: The cytotoxicity effect of I-OTB was comparable to that of OTB. This result indicates that the iodine substituent in OTB did not alter the parent compound selectivity toward double mutations EGFR L858R/T790M. Therefore, I-OTB is prominent for radioiodination, and [$^{123/124}$I] I-OTB may be a promising candidate for EGFR L858R/T790M mutation imaging.

Introduction

Various imaging radiopharmaceuticals with positron emission tomography (PET) or single-photon emission computed tomography (SPECT) are essential in precision medicine.[1,2] These techniques are noninvasive and provide quantitative details of biological functions with high sensitivity. Furthermore, in response to limitations found in an invasive biopsy limitation and in response to any bias resulting from tumor heterogeneity,[3,4] molecular imaging employing PET or SPECT can stratify patients based

*Corresponding authors: Muammar Fawwaz, Email: muammar.fawwaz@umi.ac.id; Kenji Mishiro, Email: mishiro@p.kanazawa-u.ac.jp; Kazuma Ogawa, Email: kogawa@p.kanazawa-u.ac.jp

on their susceptibilities to various diseases and may be classified into the genetic, molecular, or cellular profiles.[5]

The imaging probes labeled with radioiodine are of great attraction because of the availability of several radioiodine isotopes, such as ^{123}I with a half-life ($t_{1/2}$) of 13.2 hours for SPECT imaging, ^{131}I with $t_{1/2}$ of 8.0 days for radionuclide therapy, and ^{124}I with $t_{1/2}$ of 4.2 days for PET imaging, also ^{125}I for various preclinical types of research and auger therapy.[6-10]

Radioiodination of tyrosine kinase inhibitors (TKIs) for imaging non-small cell lung cancer (NSCLC) has attracted a lot of scientists' attention due to their unique interaction with the target epidermal growth factor receptor (EGFR).[11-14] So far, various TKI imaging probes have been developed to assess the EGFR mutation status in NSCLC. However, the radiotracers employed in the imaging of double mutations of EGFR T790M/L858R, such as [^{11}C]osimertinib, [^{11}C]rociletinib, [^{125}I]ICO1686, [^{77}Br]BrCO1686, [^{125}I]I-osimertinib, and [^{77}Br]Br-osimertinib have some limitations, such as low accumulation in the targeted tumor, which results in insufficient tumor-to-blood ratios or tumor-to-nontarget tissue ratios.[11-13,15]

Olmutinib (Olita™, OTB, Fig. 1) is one of the orally active third-generation TKIs and selectively inhibits the EGFR with L858R and T790M mutations, sparing a wild type of EGFR.[16,17] In 2016, it was approved to treat some NSCLC patients suffering from double mutations EGFR L858R/T790M in South Korea.[16,18] The chemical structure of OTB contains three crucial functional groups, namely, the pyrimidine group, *N*-methyl piperazine ring, and acrylamide group (Fig. 2).[19,20] The pyrimidine is essential for binding to an ATP binding site in the EGFR.[21] Considering the anticipated effect on the affinity to the EGFR and synthetic accessibility, we aimed to estimate the interaction of the iodinated OTB (I-OTB)-receptor complex by molecular docking. Furthermore, we will synthesize the novel I-OTB and evaluate its activity toward EGFR L858R/T790M by *in vitro* cytotoxicity assay.

Here, a novel non-radioactive iodinated *N*-{3-iodo-5-[(2-{[4-(4-methylpiperazin-1-yl)phenyl]amino}thieno{3,2-d}pyrimidin-4-yl)oxy]phenyl} (I-OTB, **11**) (Fig. 2) was synthesized. Moreover, EGFR subtype specificity of I-OTB was evaluated by employing three kinds of human NSCLC cell lines, namely H1975 (double mutations EGFR L858R/T790M), H3255 (active mutant EGFR L858R), and H441 (wild-type). This preliminary study is for developing a radioiodinated probe for companion diagnosis to select patients with the third generation of EGFR-TKIs.

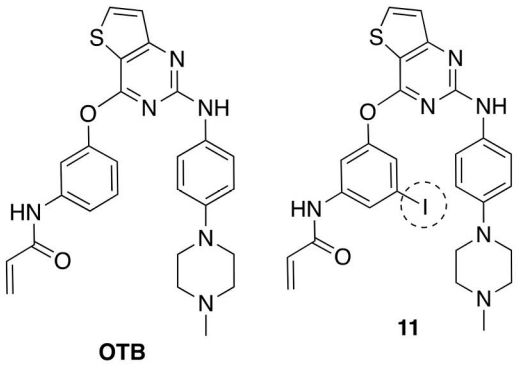

Fig 1. Structural formula of OTB and 11.

Materials and Methods

Chemicals

Trypsin-ethylenediaminetetraacetic acid (EDTA) 0.25%, phosphate-buffered saline (PBS), penicillin-streptomycin (PS), Dulbecco's Modified Eagle Medium (DMEM)/Ham's F-12 and RPMI-1640 medium were acquired from Nacalai Tesque, Inc. (Kyoto, Japan). Fetal bovine serum (FBS) was obtained from Biowest (Nuaillé, France). Solvents and reagents were purchased from Nacalai Tesque, Inc. (Kyoto, Japan), Merck (Darmstadt, Germany), Fujifilm Wako (Osaka, Japan), Kanto Chemical, Co., Inc. (Tokyo, Japan), and Tokyo Chemical Industry, Co., Ltd. (Tokyo, Japan).

Instrumentations

Auto Gamma System ARC-7010B (Hitachi, Ltd., Tokyo, Japan) recorded radioactivity. Thin-layer chromatography (TLC) on silica plates 60 F254 (Merck, Darmstadt, Germany) was used to monitor the reactions. High-performance liquid chromatography (HPLC) of SPD-20A system (Shimadzu Corp., Kyoto, Japan), using a Cosmosil® 5SL-II (20 ID × 250 mm) column (Nacalai Tesque, Inc., Kyoto, Japan). Nuclear magnetic resonance (NMR) spectroscopy was conveyed on JNM-ECS 400 and JNM-ECA 600 (JEOL Ltd., Tokyo, Japan). Direct analysis in real-time mass spectrometry (DART-MS) and electrospray ionization mass spectrometry (ESI-MS) were conducted on JMS-T100TD (JEOL Ltd., Tokyo, Japan). The optical density in 2-(2-methoxy-4-nitrophenyl)-3-(4-nitrophenyl)-5-(2,4-disulfophenyl)-2H tetrazolium monosodium salt (WST-8) assay was conducted on Infinite® F200 Pro microplate reader (TECAN, Männedorf, Switzerland).

Molecular docking

In this current study, molecular docking was performed using the AutoDock Vina package to estimate the interaction of the ligand-receptor complex.[22] The ligand molecule of OTB was retrieved from the PubChem database (CID: 54758501). The ligand was downloaded and saved to sdf extension. Meanwhile, a structure of **11** was generated by substituting a hydrogen atom in an aromatic ring of OTB with an iodine atom using MarvinSketch program packages. The structure was converted to 3D and saved to a protein data bank (PDB) file. Then, we applied Open Babel 2.4.1 program packages to convert sdf and pdb files to pdbqt formats.[23] The chemical structures of these ligands are shown in Fig. 1.

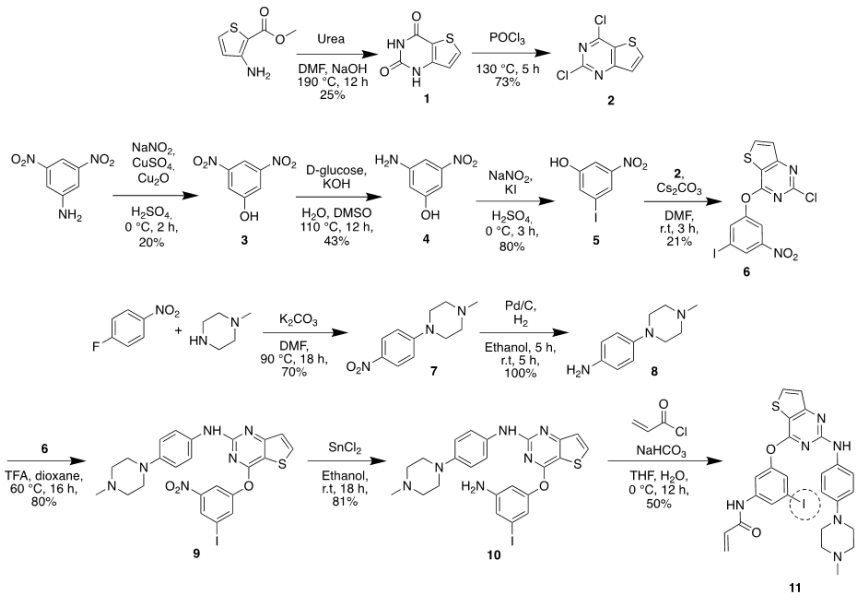

Fig. 2. Synthetic scheme of iodinated compound 11.

In receptor preparation, the three-dimensional structure of EGFR was obtained from the RCSB database (PDB ID: 3ika) (Fig. 3). The polar hydrogen and Kollman's united atom charges were computed to the receptor. Afterward, the receptor was saved in pdbqt format. All the docking results were processed and visualized in Open-Source PyMOL v 2.3 software.[24]

To perform molecular docking, the grid box parameter was required to limit the position and conformation of the ligand around the receptor site. The grid box was set on 24 × 22 × 22 with a grid spacing of 1.00 Å. Meanwhile, the grid box center was assigned at the coordinates -3.764 × 21.197 × 30.443. The exhaustiveness was computed at 100. Other parameters were computed as the default of AutoDock Vina. The Broyden-Fletcher-Goldfarb-Shanno (BFGS) algorithm was utilized as a search parameter. All parameters were set using AutoDock Tools 1.5.6 created by Morris and co-workers.[25] The docking parameters were computed according to similar protocols to our previous works.[26-28]

Probe synthesis

Fig. 2 shows the synthesis procedures of **11**,[12,29-31] and Supplementary file 1 (Figures S1-S12) supplies the ^{1}H

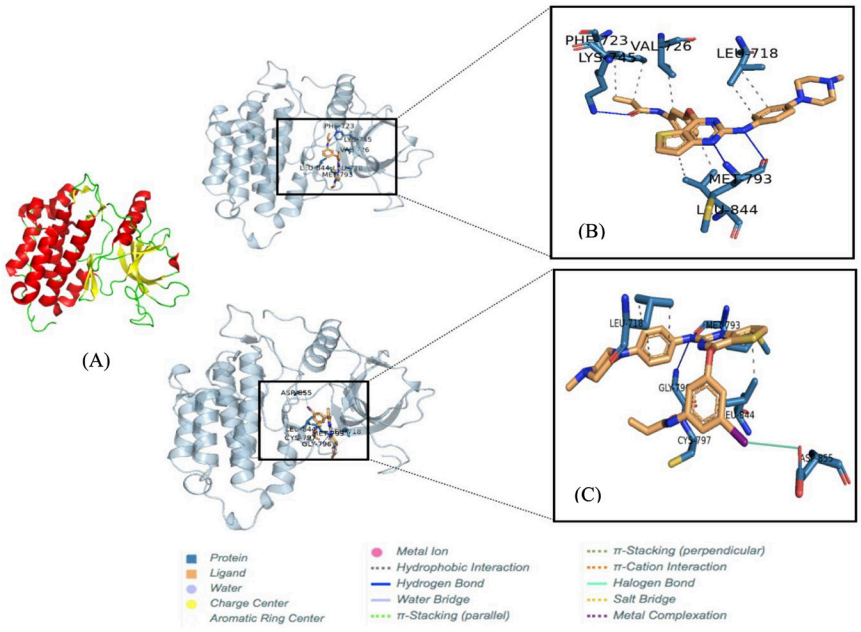

Fig. 3. The tertiary structure of EGFR T790M. The alpha-helix and beta-sheet structures are presented by red and yellow colors in cartoon models, respectively (A). The binding poses between ligand and receptor (B) OTB (C) 11. The conformation pose of each complex was visualized by PLIP program combined with Pymol v 2.3 program packages.

NMR spectra of all intermediate compounds and the final product. Additionally, the MS spectra and HPLC chromatogram confirmed the final product.

Synthesis of thieno(3,2-d)pyrimidine-2,4(1H,3H)-dione (1)

To a stirred mixture of methyl 3-aminothiophene-2-carboxylate ($C_6H_7NO_2S$) (200 mg, 1.27 mmol, 1 eq.) and *N,N*-dimethylformamide (DMF) (500 µL), urea (450 mg, 7.62 mmol, 6 eq.) was added, and the mixture was continued stirring at 190 °C for 12 hours in a sealed tube. The reaction mixture was cooled to room temperature after the reaction was completed. After that, to the reaction mixture, 1 M aqueous sodium hydroxide (NaOH) solution was added, and insoluble material was removed by suction filtration. The filtrate was neutralized using 1 M aqueous hydrochloric acid (HCl) solution. The reaction mixture was extracted with ethyl acetate. The organic phase was separated, dried using sodium sulfate (Na_2SO_4), filtered, and concentrated by a rotary evaporator to afford **1** (50 mg, 25%) as a grey solid. ^{1}H NMR (400 MHz, $(CD_3)_2SO$): δ 6.91 (1H, d, *J* = 5.2 Hz), 8.04 (1H, d, *J* = 4.8 Hz), 11.23 (1H, s), 11.57 (1H, s). MS (DART–) calculated for $C_6H_4N_2O_2S$ $[M–H]^-$: *m/z* = 167.0, found 167.6.

Synthesis of 2,4-dichlorothieno(3,2-d)pyrimidine ***(2)***

The mixture of **1** (30 mg, 0.17 mmol, 1 eq.) and phosphorus oxychloride ($POCl_3$) (200 µL) was stirred at 130 °C for 5 hours. The reaction mixture was cooled to room temperature after the reaction was completed. After that, to the reaction mixture, distilled water was added. The mixture was extracted with ethyl acetate, and the organic phase was separated, dried with Na_2SO_4, filtered, and concentrated by a rotary evaporator to afford **2** (22 mg, 73%) as a pale yellow solid. ^{1}H NMR (400 MHz, $CDCl_3$): δ 7.56 (1H, d, *J* = 5.2 Hz), 8.13 (1H, d, *J* = 6.0 Hz). MS (DART–) calculated for $C_6H_2Cl_2N_2S$ $[M–H]^-$: *m/z* = 202.9, found 202.9.

Synthesis of 3,5-dinitrophenol ***(3)***

To a stirred mixture of 3,5-dinitroaniline ($C_6H_5N_3O_4$) (91 mg, 0.5 mmol, 1.0 eq.) and sulfuric acid (H_2SO_4) (80 µL, 1.5 mmol, 3 eq.), sodium nitrite ($NaNO_2$) in water 3 mL (38 mg, 0.55 mmol, 1.1 eq.) was added at 0 °C. TLC monitored the reaction to ensure the formation of the diazonium salt. Then saturated aqueous copper (II) sulfate ($CuSO_4$) (50 mL) was added to the mixture, followed by the addition of copper (I) oxide (Cu_2O) (72 mg, 0.5 mmol, 1 eq.). The mixture was stirred at room temperature for 2 hours. After the reaction was completed, the reaction mixture was neutralized with saturated aqueous sodium bicarbonate ($NaHCO_3$). The mixture was extracted with ethyl acetate, and the organic phase was separated, dried with Na_2SO_4, filtered, and concentrated by a rotary evaporator. The residue was purified by column chromatography on silica gel (eluent: hexane/ethyl acetate = 7/3) to afford **3** (18 mg, 20%) as a pale yellow solid. ^{1}H NMR (400 MHz, $CDCl_3$): δ 6.69 (1H, s), 8.02 (2H, d, *J* = 2.0 Hz), 8.63 (1H, t, *J* = 2.0 Hz). MS (DART–) calculated for $C_6H_4N_2O_5$ $[M–H]^-$: *m/z* = 183.0, found 183.7.

Synthesis of 3-amino-5-nitrophenol ***(4)***

To a stirred solution of **3** (5 mg, 0.05 mmol, 1.0 eq.) in H_2O/DMSO (1/1) (400 µL), potassium hydroxide (KOH) (6 mg, 0.21 mmol, 4 eq.) and D-glucose (10 mg, 0.1 mmol, 2 eq.) were added at room temperature. The mixture was stirred at 110 °C for 12 hours. The mixture was cooled to room temperature and extracted with ethyl acetate. The organic phase was separated, dried with Na_2SO_4, filtered, and concentrated by a rotary evaporator. The residue was purified by column chromatography on silica gel (eluent: chloroform) to afford **4** (2 mg, 43%) as a pale yellow solid. ^{1}H NMR (400 MHz, $(CD_3)_2SO$): δ 7.67 (1H, t, *J* = 2.4 Hz), 7.85 (2H, s), 8.06 (1H, t, *J* = 2.4 Hz), 8.42 (2H, td, *J* = 7.6, 1.6 Hz). MS (DART–) calculated for $C_6H_6N_2O_3$ $[M–H]^-$: *m/z* = 153.0, found 153.4.

Synthesis of 3-iodo-5-nitrophenol ***(5)***

To a stirred mixture of **4** (30 mg, 0.19 mmol, 1.0 eq.) and H_2SO_4 (30 µL), $NaNO_2$ in water 1 mL (20 mg, 0.29 mmol, 1.5 eq.) was added at 0 °C for 3 hours. The reaction was monitored by TLC to ensure the formation of the diazonium salt, and then potassium iodide (KI) (80.51 mg, 0.48 mmol, 2.5 eq.) was added to the mixture at room temperature. After 3 hours, The reaction mixture was neutralized using saturated aqueous $NaHCO_3$. The mixture was extracted with ethyl acetate, and the organic phase was separated, dried with Na_2SO_4, filtered, and concentrated by a rotary evaporator. The residue was purified with column chromatography on silica gel (eluent: chloroform) to afford **5** (41 mg, 80%) as a pale yellow solid. ^{1}H NMR (400 MHz, $(CDCl_3)$: δ 5.54 (1H, s), 7.54 (1H, dd, *J* = 2.4, 1.2 Hz), 7.66 (1H, t, *J* = 2.4 Hz), 8.14 (1H, t, *J* = 2.0 Hz). MS (DART–) calculated for $C_6H_4INO_3$ $[M–H]^-$: *m/z* = 263.9, found 263.9.

Synthesis of 2-chloro-4-(3-iodo-5-nitrophenoxy)thieno(3,2-d)pyrimidine ***(6)***

To a stirred mixture of **2** (24 mg, 0.11 mmol, 1 eq.) and DMF (1 mL), **5** (29 mg, 0.11 mmol, 1 eq.), and cesium carbonate (Cs_2CO_3) (71 mg, 0.22 mmol, 2 eq.) were added at room temperature. The mixture was stirred at room temperature for 3 hours, and the reaction was monitored by TLC. The reaction mixture was quenched with water and then extracted with ethyl acetate. The organic phase was separated, dried with Na_2SO_4, filtered, and concentrated by a rotary evaporator. The residue was purified by column chromatography on silica gel (eluent: chloroform) to afford **6** (10 mg, 21%) as a pale yellow solid. ^{1}H NMR (400 MHz, $(CDCl_3)$: δ 7.55 (1H, d, *J* = 5.6 Hz), 8.00 (1H, s), 8.08 (1H, d, *J* = 4.0 Hz), 8.17 (1H, t, *J* = 1.6 Hz), 8.54 (1H, s). MS (DART+) calculated for $C_6H_5INO_3$ $[M+H]^+$: *m/z* = 433.9, found 433.7.

Synthesis of 1-methyl-4-(4-nitrophenyl)piperazine ***(7)***

To a stirred mixture of 1-methylpiperazine ($C_5H_{12}N_2$) (0.61 mL, 5.45 mmol) in DMF (6.25 mL), 4-fluoronitrobenzene ($C_6H_4FNO_2$) (0.75 ml, 7.07 mmol) and potassium carbonate (K_2CO_3) (1.13 g, 8.18 mmol) were added, and the mixture was stirred at 90 °C for 18 hours. The mixture

was cooled to room temperature and extracted with ethyl acetate. The organic phase was separated, dried with Na_2SO_4, filtered, and concentrated by a rotary evaporator. The residue was purified by column chromatography on silica gel (eluent: chloroform) to afford **7** (1.1 g, 70%) as a yellow solid. ^{1}H NMR (400 MHz, $CDCl_3$): δ 2.36 (3H, s), 2.56 (4H, t, *J* = 5.6 Hz), 3.44 (4H, t, *J* = 5.6 Hz), 6.82 (2H, dt, *J* = 9.6, 2.4 Hz), 8.12 (2H, dt, *J* = 9.6, 2.4 Hz). MS (DART+) calculated for $C_{11}H_{15}N_3O_2$ $[M+H]^+$: *m/z* = 222.1, found 222.1.

Synthesis of 4-(4-methylpiperazin-1-yl)aniline ***(8)***

To a stirred mixture of **7** (100 mg, 0.45 mmol, 1.0 eq.) and ethanol (4.50 mL), palladium on carbon (Pd/C 10%) (24 mg) was added under a nitrogen atmosphere. The nitrogen was exchanged with hydrogen, and the mixture was stirred under the hydrogen atmosphere (1 atm) for 5 hours. The mixture was filtrated through a pad of Celite® to remove the catalyst, and a rotary evaporator concentrated the filtrate to afford **8** (98 mg, 100%) as a purple solid. ^{1}H NMR (400 MHz, ($CDCl_3$): δ 2.34 (3H, s), 2.58 (4H, t, *J* = 4.8 Hz), 3.07 (4H, t, *J* = 4.8 Hz), 6.65 (2H, dt, *J* = 9.2, 2.4 Hz), 6.81 (2H, dt, *J* = 8.4, 1.6 Hz). MS (DART+) calculated for $C_{11}H_{17}N_3$ $[M+H]^+$: *m/z* = 192.1, found 192.0.

Synthesis of 4-(3-nitro-5-iodophenoxy)-N-[4-(4-methylpiperazin-1-yl)phenyl]thieno(3,2-d)pyrimidin-2-amine ***(9)***

To a stirred mixture of **6** (10 mg, 0.02 mmol) and 2.0 M trifluoroacetic acid (TFA)/dioxane (200 µL), **8** (4.4 mg, 0.02 mmol) was added, and the mixture was stirred at 60 °C for 16 hours. The reaction mixture was neutralized with saturated aqueous $NaHCO_3$ and extracted with ethyl acetate. The organic phase was separated, dried with Na_2SO_4, filtered, and concentrated by a rotary evaporator. The residue was purified by column chromatography on silica gel (eluent: chloroform) to afford **9** (9.3 mg, 80%) as a yellow solid. ^{1}H NMR (400 MHz, $CDCl_3$): δ 2.38 (3H, s), 2.63 (4H, t, *J* = 5.0 Hz), 3.18 (4H, t, *J* = 5.0 Hz), 6.80–6.85 (3H, m), 7.28 (1H, d, *J* = 5.6 Hz), 7.33 (1H, d, *J* = 8.8 Hz), 7.87 (1H, d, *J* = 5.6 Hz), 8.01 (1H, t, *J* = 1.8 Hz), 8.16 (1H, t, *J* = 2.0 Hz), 8.50 (1H, t, *J* = 1.8 Hz). MS (DART+) calculated for $C_{23}H_{21}IN_6O_3S$ $[M+H]^+$: *m/z* = 589.0, found 588.8.

Synthesis of 4-(3-amino-5-iodophenoxy)-N-[4-(4-methylpiperazin-1-yl)phenyl]thieno(3,2-d)pyrimidin-2-amine ***(10)***

To a stirred mixture of **9** (13 mg, 0.02 mmol, 1 eq.) and ethanol (2.0 mL), $SnCl_2$ (39.7 mg) was added under a nitrogen atmosphere at room temperature. After stirring for 18 hours, the reaction mixture was neutralized with saturated aqueous $NaHCO_3$ and extracted with ethyl acetate. The organic phase was separated, dried with Na_2SO_4, filtered, and concentrated by a rotary evaporator to afford **10** (10 mg, 81%) as a yellow solid. ^{1}H NMR (400 MHz, $CDCl_3$): δ 2.36 (3H, s), 2.59 (4H, t, *J* = 4.4 Hz), 3.16 (4H, t, *J* = 4.8), 6.55 (1H, t, *J* = 1.6 Hz), 6.88 (1H, s), 6.89 (1H, d, *J* = 9.2 Hz), 6.99 (1H, td, *J* = 1.6, 2.0 Hz), 7.04 (1H, t, *J* = 1.6 Hz), 7.25 (1H, d, 5.6 Hz), 7.42 (1H, d, *J* = 8.8 Hz), 7.81 (1H, t, *J* = 4.8 Hz). MS (ESI+) calculated for $C_{23}H_{23}IN_6OS$ $[M+H]^+$: *m/z* = 559.1, found 559.2.

Synthesis of N-{3-iodo-5-[(2-{[4-(4-methylpiperazin-1-yl)phenyl]amino}thieno{3,2-d}pyrimidin-4-yl)oxy]phenyl} ***(11)***

To a stirred mixture of **10** (5 mg, 0.01 mmol, 1.0 eq.), *N,N*-Diisopropylethylamine (DIPEA) (20 µL), and dichloromethane (DCM) (300 µL), acryloyl chloride (0.72 µL, 0.01 mmol, 1.0 eq.) was added at −30 °C and the mixture was stirred for 2 hours. The crude product was purified by HPLC with mobile phase system chloroform/methanol = 9/1, using a Cosmosil® 5SL-II (20 ID × 250 mm) column, flow rate 9.5 mL/min to afford **11** (1.1 mg, 10%) as a pale yellow solid. ^{1}H NMR (400 MHz, $CDCl_3$): δ 2.42 (3H, s), 2.65 (4H, br, s), 3.19 (4H, br, s), 5.80–6.70 (3H, m), 6.80–6.85 (3H, m)[a], 7.29 (1H, d, *J* = 4.8 Hz), 7.33 (2H, d, *J* = 8.0 Hz), 7.56 or 7.78 (1H, s)[b], 7.88 (1H, d, *J* = 5.2 Hz), 8.01 (1H, t, *J* = 1.6 Hz), 8.16 (1H, t, *J* = 2.0 Hz), 8.50 (1H, t, *J* = 2.0 Hz). MS (ESI+) calculated for $C_{26}H_{25}IN_6O_2S$ $[M+H]^+$: *m/z* = 613.1, found 613.2. [a]Three protons derived from an impurity are also observed in this area. [b]One of these two singlet signals is derived from an impurity.

Cytotoxicity assays

The half inhibitory concentration (IC_{50}) of **11** and OTB toward NSCLC cell lines (H1975, H3255, and H441) was determined by WST-8 assay. These cell lines were kindly provided by Dr. Juri G. Gelovani, formerly of the Department of Experimental Diagnostic Imaging at the University of Texas, MD Anderson Cancer Center, Houston, TX., USA. The cells were seeded in a medium enriched with 10% FBS and 100 IU/mL PS in 96-well culture plates. The cells were allowed to reach a density of 2.5×10^3 cells/well (H1975 and H441) and 1×10^4 cells/well (H3255) by incubated for 24 h, 5% CO_2, at 37 °C. After incubation, concentrations (0.01–100 µM) of **11** or OTB treated the cells for 48 h, and the Cell Counting Kit-8 (Dojindo, Kumamoto, Japan) assessed cell viability following the manufacturer's protocol.

Statistical analysis

The data were statistically analyzed by unpaired Student's *t*-test using GraphPad Prism 8.4.3 software (GraphPad Software, San Diego, CA, USA). All values are presented as mean ± standard deviation (SD), and $P < 0.05$ was considered statistically significant.

Results

Molecular docking

A molecular docking simulation was carried out to explore the binding mode of compound **11** to the active site of EGFR T790M (PDB code: 3ika). The binding energy of OTB and **11** in complex with EGFR T790M are –8.7 and –7.9 kcal/mol, respectively. These results indicate that the energy required for OTB and **11** to bind to the target receptor is similar. Thus, the modification of **11** does not affect its

affinity for the T790M. Fig. 3 visualizes the binding pose of ligands at the site of the receptor. Moreover, Tables 1 and 2 summarize the detailed information on the ligand-receptor interactions by hydrogen and hydrophobic bond, respectively.

Probe synthesis

According to the reported crystal structure, the essential substituents playing a vital role in the binding of OTB to EGFR L858R/T790M are the pyrimidine group, *N*-methyl piperazine ring, and acrylamide group.[19,20] We hypothesized that compound **11**, having an iodine atom at C(5) of the phenyl group in the 3-aryloxyanilide structure of OTB, could retain the original affinity of OTB toward EGFR L858R/T790M. A derivative of OTB, an iodinated compound of **11,** was prepared by conducting several multistep reactions starting from a commercially-available material based on the reported procedure.[12,29-31]

Cytotoxicity assays

The IC_{50} of **11** was determined by employing a WST-8 assay. Although the cytotoxicity of **11** against H1975 was a little less than OTB, as shown in Table 3, the selectivity of **11** toward dual mutations EGFR cell line (H1975) was better than the parent compound, OTB.

Discussion

Several radiolabeled EGFR TKIs have been developed to serve as imaging agents to create therapeutic effects in the TKIs therapy for NSCLC. Some have been developed to monitor tumors using an EGFR L858R or EGFR del19.[32,33] However, most agents did not show satisfactory results when stratifying the NSCLC patients with double mutations of EGFR L858R/T790M.[34] Therefore, various scientists have continued their studies to develop a genuinely-effective imaging agent employed to diagnose and stratify the NSCLC patients with EGFR L858R/T790M regarding their therapeutic response to TKIs.

To overcome the TKI resistance caused by the T790M mutation, the third-generation TKIs were designed to possess a hydrophobic part that binds to a hydrophobic pocket modified by the mutation.[35] Additionally, the

Table 1. Hydrogen bonds of ligands in complex with the receptor

Model	Residue	AA	Distance H-A (Å)	Distance D-A (Å)	Donor angle	Donor atom	Acceptor atom
OTB	745	LYS	1.90	2.82	147.40	470 [N]	6025 [O_2]
	793	MET	2.21	3.06	139.93	6001 [N]	904 [O_2]
	793	MET	2.24	3.21	160.17	900 [N]	5993 [N_2]
11	793A	MET	1.83	2.80	171.38	6001 [N]	904 [O_2]
	793A	MET	2.25	3.21	155.29	900 [N]	5993 [N_2]
	796A	GLY	3.36	3.97	120.13	928 [N]	6001 [Npl]
	797A	CYS	2.67	3.34	123.70	933 [N]	6027 [O_2]

Table 2. Hydrophobic interactions of ligands in complex with receptor

Model	Residue	AA	Distance	Ligand atom	Protein atom
OTB	718A	LEU	3.95	6007	228
	718A	LEU	3.82	6008	230
	723A	PHE	3.75	6027	266
	723A	PHE	3.80	6028	262
	726A	VAL	3.75	6018	288
	844A	LEU	3.60	6022	1432
	844A	LEU	3.38	5999	1431
11	718A	LEU	3.73	6007	228
	718A	LEU	3.75	6008	230
	718A	LEU	3.56	6005	231
	844A	LEU	3.24	5999	1431

Table 3. The IC_{50} of **11**, OTB, and gefitinib toward NSCLC cell lines by WST-8 assay

Cells lines	Mutation status	IC_{50} (μM)		
		11	OTB	Gefitinib*
H1975	L858R/T790M	10.49 ± 5.64	5.67 ± 2.19	> 10
H3255	L858R	14.55 ± 1.62	1.23 ± 1.23	0.02 ± 0.02
H441	Wild type	> 10	> 10	> 10

Data represent the mean ± SD of three separate experiments.
*Data from reference Fawwaz et al.[12]

acrylamide group was employed to form a covalent bond with the thiol of cysteine 797, resulting in irreversible inhibition of the EGFR.[36] Many studies have shown that OTB selectively inhibits EGFR with mutations, especially the double mutations of L858R/T790M. In addition, OTB has fewer adverse effects, such as gastrointestinal toxicity, compared to first-generation and second-generation TKIs.[18] Owing to the high selectivity of OTB, we hypothesized that a radioiodinated variant of OTB could overcome the limitation observed in the previously developed imaging agents for EGFR double mutations. Because the iodinated variant is required to retain the high selectivity of OTB, the iodine atom should be introduced into a structure such as a phenyl group in the 3-aryloxyanilide structure, which does not essentially participate in binding to the EGFR.[7,37]

The docking study showed that **11** has an interaction similar to that of the parent compound OTB with the EGFR T790M mutation. The estimated binding energy of **11** toward the EGFR was comparable to that of OTB. As seen in many EGFR kinase inhibitors,[35] the pyrimidine ring is the most important group. Thus, we choose the best binding pose depending on the lowest binding energy between the ligand and the receptor by considering the position of the pyrimidine. In addition, the interaction between the ligand and the receptor by hydrogen and hydrophobic binding is also considered.

Both compounds exhibited hydrogen bonds with Met-793 in the hinge region (Table 1 and Fig. 3). The hydrophobic interaction of the thienopyrimidine group with a hydrophobic pocket composed of Ala-743, Met-790, and Leu-844 was also essential for binding the ligand and the EGFR T790M (Table 2). This result supported an experimental finding that a molecule associating with the Met-790 in an ATP-binding pocket of the T790M EGFR is critical for overcoming T790M EGFR drug resistance to first- and second-generation EGFR TKIs.[35] Additionally, the diaminophenyl group showed hydrophobic interaction with Leu-718. In the found conformation, the acrylamide group was located at a position appropriate for the Michael addition by thiol in Cys-797. Unexpectedly, the introduced iodine showed a halogen bond interaction with Asp-855; hence, substituting iodine at this position could increase affinity **11** toward EGFR.

The synthesis of **11** was conducted by employing multistep reactions starting from a commercially-available material. In the final product analysis using NMR, several peaks arise in the chemical shift corresponding to protons in the chemical structure **11**. The characteristic peak **11** was similar to OTB's, wherein protons bound to the aromatic and alkyl groups in both compounds appear in the downfield and upfield areas, respectively. The peak in the piperazine group appeared in the same chemical shift at 2.65 – 3.19 ppm.

To support the molecular docking research, it was necessary to study the cytotoxic activity *in vitro*. In this study, three different kinds of human NSCLC cell lines such as H1975 (EGFR L858R/T790M mutation), H3255 (EGFR L858R active mutant), and H441 (wild type EGFR) were employed. Although the IC_{50} of **11** toward double mutations EGFR was less than OTB (Table 3), **11** showed selectivity toward EGFR L858R/T790M compared to OTB. The decrease in activity **11** against H1975 was not necessarily caused by iodination but could be caused by impurities that contaminated the product. After HPLC purification, the data from the HPLC chromatogram, ^{1}H NMR spectrum, and ESI-MS spectrum indicated the presence of **11** as a major compound. However, ^{1}H NMR spectrum indicated contamination with almost an equimolar amount of acrylamide-related impurity (Fig. S11). To confirm the precise activity of **11**, further purification or improvement of the synthetic procedure is required.

The cytotoxicity of **11** toward cancer cells with double mutations of EGFR was higher than that of gefitinib. Moreover, the IC_{50} of gefitinib toward H3255 as EGFR L858R was lower than **11**. Since the cytotoxicity of all compounds toward H441 was not observed, we could prove that **11** and gefitinib had a high selectivity towards the EGFR L858R/T790M mutations and EGFR L858R, respectively. These data indicated that the iodine substituent in OTB increased selectivity toward H1975 and decreased activity against H3255. These characteristics served as a positive value for **11** and proved beneficial to **11** since they could improve the contrast in the imaging application and facilitate the stratification of the mutation status.

The biodistribution profile of OTB in the human body exhibited its rapid absorption and distribution into the organs. Moreover, OTB showed a fast plasma clearance and was excreted via the kidney in intact form.[38] These characteristics are suitable for a radiotracer. Considering its high selectivity toward the L858R/T790M double mutations of EGFR compared to the wild-type EGFR and its fast plasma clearance, we expected that **11** would highly accumulate in the targeted tumor with EGFR L858R/T790M mutations. Therefore, we are strongly encouraged to conduct research using a radioiodinated variant of **11** since it is expected to show similar *in vivo* characteristics to OTB.

Conclusion

The OTB analog, **11**, was successfully synthesized by multistep reactions. The molecular docking and *in vitro* cytotoxicity assays indicated that **11** has higher cytotoxicity and affinity towards the EGFR L858R/T790M mutation than wild-type EGFR. Therefore, we prove that introducing iodine into OTB does not alter the parent compound's selectivity toward double mutations EGFR L858R/T790M. Therefore, [$^{123/124}$I]I-OTB, the radioiodinated variant of **11**, could be a promising candidate for EGFR L858R/T790M mutation imaging.

Research Highlights

What is the current knowledge?

√ OTB is the TKIs' third generation, selectively inhibiting the activated double mutation EGFR L858R/T790M in lung cancer.

What is new here?

√ The OTB derivative was successfully synthesized and showed high selectivity toward EGFR L858R/T790M mutation compared to EGFR L858R and wild-type.

Acknowledgments

This work was supported by Terumo Life Science Foundation and MEXT KAKENHI Grant-in-Aid for Scientific Research (16H05397). The authors greatly acknowledge the Ministry of Research, Technology and Higher Education, Indonesia, along with the Institute of Research and Resource Development (LP2S), Universitas Muslim Indonesia, Makassar, Indonesia, for supporting the finalization of this study.

Authors' Contribution

Conceptualization: Muammar Fawwaz, Kazuma Ogawa, Kenji Mishiro, Ryuichi Nishii.
Data curation: Muammar Fawwaz, Kazuma Ogawa, Kenji Mishiro.
Formal analysis: Muammar Fawwaz, Kazuma Ogawa, Kenji Mishiro, Arwansyah.
Funding acquisition: Muammar Fawwaz, Kazuma Ogawa.
Investigation: Muammar Fawwaz, Kazuma Ogawa, Kenji Mishiro, Arwansyah.
Methodology: Muammar Fawwaz, Kazuma Ogawa, Kenji Mishiro, Ryuichi Nishii, Arwansyah.
Project administration: Muammar Fawwaz, Kazuma Ogawa.
Resources: Muammar Fawwaz, Kazuma Ogawa, Kenji Mishiro, Ryuichi Nishii.
Software: Muammar Fawwaz, Arwansyah.
Supervision: Kazuma Ogawa, Kenji Mishiro.
Validation: Muammar Fawwaz, Kazuma Ogawa, Kenji Mishiro.
Visualization: Muammar Fawwaz, Kazuma Ogawa, Kenji Mishiro.
Writing–original draft: Muammar Fawwaz, Kazuma Ogawa, Kenji Mishiro.
Writing–review & editing: Muammar Fawwaz, Kazuma Ogawa, Kenji Mishiro.

Competing Interests

The authors declare no conflicts of interest.

Data Availability Statement

The data that supports the findings of this study are available in the supplementary material of this article.

Ethical Statement

The authors declare no ethical issues to be considered.

Supplementary files

Supplementary file 1 contains Figs. S1-S12.

References

1. Manning HC. World Molecular Imaging Congress 2015: precision medicine visualized. *Mol Imaging Biol* **2015**; 17: 295-6. https://doi.org/10.1007/s11307-015-0855-3
2. Waaijer SJH, Kok IC, Eisses B, Schröder CP, Jalving M, Brouwers AH, *et al.* Molecular Imaging in Cancer Drug Development. *J Nucl Med* **2018**; 59: 726-32. https://doi.org/10.2967/jnumed.116.188045.
3. Peled N, Roisman LC, Miron B, Pfeffer R, Lanman RB, Ilouze M, *et al.* Subclonal Therapy by Two EGFR TKIs Guided by Sequential Plasma Cell-free DNA in EGFR-Mutated Lung Cancer. *J Thorac Oncol* **2017**; 12: e81-e4. https://doi.org/10.1016/j.jtho.2017.02.023
4. Tan DS, Yom SS, Tsao MS, Pass HI, Kelly K, Peled N, *et al.* The International Association for the Study of Lung Cancer Consensus Statement on Optimizing Management of EGFR Mutation-Positive Non-Small Cell Lung Cancer: Status in 2016. *J Thorac Oncol* **2016**; 11: 946-63. https://doi.org/10.1016/j.jtho.2016.05.008
5. Sun X, Xiao Z, Chen G, Han Z, Liu Y, Zhang C, *et al.* A PET imaging approach for determining EGFR mutation status for improved lung cancer patient management. *Sci Transl Med* **2018**; 10: 1-13. https://doi.org/10.1126/scitranslmed.aan8840
6. Cavina L, van der Born D, Klaren PHM, Feiters MC, Boerman OC, Rutjes F. Design of Radioiodinated Pharmaceuticals: Structural Features Affecting Metabolic Stability towards in Vivo Deiodination. *European J Org Chem* **2017**; 2017: 3387-414. https://doi.org/10.1002/ejoc.201601638
7. Dubost E, McErlain H, Babin V, Sutherland A, Cailly T. Recent Advances in Synthetic Methods for Radioiodination. *J Org Chem* **2020**; 85: 8300-10. https://doi.org/10.1021/acs.joc.0c00644
8. Liu N, Shi Y, Guo J, Li H, Wang Q, Song M, *et al.* Radioiodinated tyrosine based carbon dots with efficient renal clearance for single photon emission computed tomography of tumor. *Nano Research* **2019**; 12: 3037-43. https://doi.org/10.1007/s12274-019-2549-7
9. Patel N, Duffy BA, Badar A, Lythgoe MF, Årstad E. Bimodal Imaging of Inflammation with SPECT/CT and MRI Using Iodine-125 Labeled VCAM-1 Targeting Microparticle Conjugates. *Bioconjug Chem* **2015**; 26: 1542-9. https://doi.org/10.1021/acs.bioconjchem.5b00380
10. Ogawa K, Takeda T, Mishiro K, Toyoshima A, Shiba K, Yoshimura T, *et al.* Radiotheranostics Coupled between an At-211-Labeled RGD Peptide and the Corresponding Radioiodine-Labeled RGD Peptide. *ACS Omega* **2019**; 4: 4584-91. https://doi.org/10.1021/acsomega.8b03679
11. Fawwaz M, Mishiro K, Nishii R, Makino A, Kiyono Y, Shiba K, *et al.* A Radiobrominated Tyrosine Kinase Inhibitor for EGFR with L858R/T790M Mutations in Lung Carcinoma. *Pharmaceuticals (Basel)* **2021**; 14: 1-14. https://doi.org/10.3390/ph14030256
12. Fawwaz M, Mishiro K, Nishii R, Sawazaki I, Shiba K, Kinuya S, *et al.* Synthesis and Fundamental Evaluation of Radioiodinated Rociletinib (CO-1686) as a Probe to Lung Cancer with L858R/T790M Mutations of Epidermal Growth Factor Receptor (EGFR). *Molecules (Basel, Switzerland)* **2020**; 25: 2914. https://doi.org/10.3390/molecules25122914
13. Mishiro K, Nishii R, Sawazaki I, Sofuku T, Fuchigami T, Sudo H, *et al.* Development of Radiohalogenated Osimertinib Derivatives as Imaging Probes for Companion Diagnostics of Osimertinib. *J Med Chem* **2022**; 65: 1835-1847. https://doi.org/10.1021/acs.jmedchem.1c01211
14. Tang L, Peng C, Tang B, Li Z, Wang X, Li J, *et al.* Radioiodinated Small-Molecule Tyrosine Kinase Inhibitor for HER2-Selective SPECT Imaging. *J Nucl Med* **2018**; 59: 1386-91. https://doi.org/10.2967/jnumed.117.205088
15. Ballard P, Yates JWT, Yang Z, Kim D-W, Yang JC-H, Cantarini M, *et al.* Preclinical Comparison of Osimertinib with Other EGFR-TKIs in EGFR-Mutant NSCLC Brain Metastases Models, and Early Evidence of Clinical Brain Metastases Activity. *Clin Cancer Res* **2016**; 22: 5130-40. https://doi.org/10.1158/1078-0432.Ccr-16-0399
16. Kim ES. Olmutinib: First Global Approval. *Drugs* **2016**; 76: 1153-7. https://doi.org/10.1007/s40265-016-0606-z
17. Lee K-O, Cha MY, Kim M, Song JY, Lee J-H, Kim YH, *et al.* Abstract LB-100: Discovery of HM61713 as an orally available and mutant EGFR selective inhibitor. *Cancer Res* **2014**; 74: LB-100-LB-. https://doi.org/10.1158/1538-7445.Am2014-lb-100
18. Kim DW, Lee DH, Han JY, Lee J, Cho BC, Kang JH, *et al.* Safety, tolerability, and anti-tumor activity of olmutinib in non-small cell lung cancer with T790M mutation: A single arm, open label, phase 1/2 trial. *Lung Cancer* **2019**; 135: 66-72. https://doi.org/10.1016/j.lungcan.2019.07.007
19. Attwa MW, Kadi AA, Abdelhameed AS. Detection and characterization of olmutinib reactive metabolites by LC–MS/MS: Elucida-

tion of bioactivation pathways. *J Sep Sci* **2020**; 43: 708-18. https://doi.org/https://doi.org/10.1002/jssc.201900818
20. Limban C, Nuţă DC, Chiriţă C, Negreş S, Arsene AL, Goumenou M, *et al.* The use of structural alerts to avoid the toxicity of pharmaceuticals. *Toxicol Rep* **2018**; 5: 943-53. https://doi.org/10.1016/j.toxrep.2018.08.017
21. Ricordel C, Friboulet L, Facchinetti F, Soria JC. Molecular mechanisms of acquired resistance to third-generation EGFR-TKIs in EGFR T790M-mutant lung cancer. *Ann Oncol* **2018**; 29: i28-i37. https://doi.org/10.1093/annonc/mdx705
22. Trott O, Olson AJ. AutoDock Vina: Improving the speed and accuracy of docking with a new scoring function, efficient optimization, and multithreading. *J Comput Chem* **2010**; 31: 455-61. https://doi.org/10.1002/jcc.21334
23. O'Boyle NM, Banck M, James CA, Morley C, Vandermeersch T, Hutchison GR. Open Babel: An open chemical toolbox. *J Cheminform* **2011**; 3: 33. https://doi.org/10.1186/1758-2946-3-33
24. Delano DL. The PyMOL Molecular Graphics System, Version 2.3. 2020. https://pymol.org/.
25. Morris GM, Huey R, Lindstrom W, Sanner MF, Belew RK, Goodsell DS, *et al.* AutoDock4 and AutoDockTools4: Automated docking with selective receptor flexibility. *J Comput Chem* **2009**; 30: 2785-91. https://doi.org/10.1002/jcc.21256
26. Arwansyah A, Arif AR, Ramli I, Kurniawan I, Sukarti S, Nur Alam M, *et al.* Molecular modelling on SARS-CoV-2 papain-like protease: an integrated study with homology modelling, molecular docking, and molecular dynamics simulations. *SAR QSAR Environ Res* **2021**; 32: 699-718. https://doi.org/10.1080/1062936X.2021.1960601
27. Arwansyah A, Arif AR, Syahputra G, Sukarti S, Kurniawan I. Theoretical studies of Thiazolyl-Pyrazoline derivatives as promising drugs against malaria by QSAR modelling combined with molecular docking and molecular dynamics simulation. *Molecular Simulation* **2021**; 47: 988-1001. https://doi.org/10.1080/08927022.2021.1935926
28. Sumaryada T, Arwansyah, Roslia AW, Ambarsari L, Kartono A, editors. Molecular docking simulation of mangostin derivatives and curcuminoid on maltase- glucoamylase target for searching anti-diabetes drug candidates. *2016 1st International Conference on Biomedical Engineering (IBIOMED)*; **2016** 5-6 Oct.
29. Kristianslund R, Vik A, Hansen TV. A convenient synthesis of phenols. *Synthetic Communications* **2018**; 48: 2809-14. https://doi.org/10.1080/00397911.2018.1496263
30. Kumar M, Sharma U, Sharma S, Kumar V, Singh B, Kumar N. Catalyst-free water mediated reduction of nitroarenes using glucose as a hydrogen source. *RSC Adv* **2013**; 3: 4894-8. https://doi.org/10.1039/C3RA40771C
31. Taniguchi T, Imoto M, Takeda M, Nakai T, Mihara M, Iwai T, *et al.* Hydrolysis of Diazonium Salts Using a Two-Phase System (CPME and Water). *Heteroatom Chemistry* **2015**; 26: 411-6. https://doi.org/10.1002/hc.21275
32. Gelovani JG. Molecular imaging of epidermal growth factor receptor expression-activity at the kinase level in tumors with positron emission tomography. *Cancer Metastasis Rev* **2008**; 27: 645-53. https://doi.org/10.1007/s10555-008-9156-5
33. Yeh HH, Ogawa K, Balatoni J, Mukhapadhyay U, Pal A, Gonzalez-Lepera C, *et al.* Molecular imaging of active mutant L858R EGF receptor (EGFR) kinase-expressing nonsmall cell lung carcinomas using PET/CT. *Proc Natl Acad Sci U S A* **2011**; 108: 1603-8. https://doi.org/10.1073/pnas.1010744108
34. Fawwaz M, Pratama M, Aminuddin AH, Baits M. Radiolabeled EGFR Tyrosine Kinase for the Detection of Dual Mutations EGFR L858R/T790M in NSCLC. *Biointerface Res Appl Chem* **2023**; 13: 1-11. https://doi.org/10.33263/BRIAC135.500
35. Yan X-E, Zhu S-J, Liang L, Zhao P, Choi HG, Yun C-H. Structural basis of mutant-selectivity and drug-resistance related to CO-1686. *Oncotarget* **2017**; 8: 53508-17. https://doi.org/10.18632/oncotarget.18588
36. Pao W, Wang TY, Riely GJ, Miller VA, Pan Q, Ladanyi M, *et al.* KRAS mutations and primary resistance of lung adenocarcinomas to gefitinib or erlotinib. *PLoS Med* **2005**; 2: 57-61. https://doi.org/10.1371/journal.pmed.0020017
37. Ogawa K, Shiba K, Akhter N, Yoshimoto M, Washiyama K, Kinuya S, *et al.* Evaluation of radioiodinated vesamicol analogs for sigma receptor imaging in tumor and radionuclide receptor therapy. *Cancer Sci* **2009**; 100: 2188-92. https://doi.org/10.1111/j.1349-7006.2009.01279.x
38. Noh YS, Yoon S, Kim SR, Lee K-T, Jang I-J. A safety, pharmacokinetic, pharmacogenomic and population pharmacokinetic analysis of the third-generation EGFR TKI, olmutinib (HM61713), after single oral administration in healthy volunteers. *Basic & Clinical Pharmacology & Toxicology* **2019**; 125: 370-81. https://doi.org/10.1111/bcpt.13262